Published in final edited form as:
Cell. 2014 December 18; 159(7): 1591–1602. doi:10.1016/j.cell.2014.11.020.

Acetate Dependence of Tumors

Sarah A. Comerford[1,7], **Zhiguang Huang**[2,7], **Xinlin Du**[2], **Yun Wang**[2], **Ling Cai**[2], **Agnes Witkiewicz**[3], **Holly Walters**[3], **Mohammed N. Tantawy**[4,5], **Allie Fu**[4], **H. Charles Manning**[4,5,6], **Jay D. Horton**[1], **Robert E. Hammer**[2], **Steven L. McKnight**[2,8], and **Benjamin P. Tu**[2,8]

[1]Department of Molecular Genetics, UT Southwestern Medical Center, Dallas, TX 75390 USA

[2]Department of Biochemistry, UT Southwestern Medical Center, Dallas, TX 75390 USA

[3]Department of Pathology, UT Southwestern Medical Center, Dallas, TX 75390 USA

[4]Vanderbilt University Institute of Imaging Science, Vanderbilt University Medical Center, Nashville, TN 37232 USA

[5]Department of Radiology and Radiological Sciences, Vanderbilt University Medical Center, Nashville, TN 37232 USA

[6]Vanderbilt-Ingram Cancer Center, Vanderbilt University Medical Center, Nashville, TN 37232 USA

SUMMARY

Acetyl-CoA represents a central node of carbon metabolism that plays a key role in bioenergetics, cell proliferation and the regulation of gene expression. How highly glycolytic or hypoxic tumors are able to produce sufficient quantities of this metabolite to support cell growth and survival under nutrient-limiting conditions remains poorly understood. Here we show that the nucleocytosolic acetyl-CoA synthetase enzyme, ACSS2, supplies a key source of acetyl-CoA for tumors by capturing acetate as a carbon source. Despite exhibiting no gross deficits in growth or development, adult mice lacking ACSS2 exhibit a significant reduction in tumor burden in two different models of hepatocellular carcinoma. ACSS2 is expressed in a large proportion of human tumors and its activity is responsible for the majority of cellular acetate uptake into both lipids and histones. These observations may qualify ACSS2 as a targetable metabolic vulnerability of a wide spectrum of tumors.

Correspondence: steven.mcknight@utsouthwestern.edu, benjamin.tu@utsouthwestern.edu.
[7]Co-first author
[8]Co-senior author

AUTHOR CONTRIBUTIONS

This study was conceived by BPT and SLM. SAC conducted the mouse breeding and in vivo liver tumorigenesis experiments, ZH, YW, LC performed the cell line experiments, XD conducted the high-throughput screen, ZH and SAC performed the IHC experiments, AW provided the collection of human triple negative breast cancers, MNT, AF, HCM performed the [^{11}C]acetate PET imaging experiments, REH, HW, JDH constructed the ACSS2 KO mice, SAC, REH, ZH, LC, BPT, SLM designed the experiments, and SAC, ZH, BPT, SLM wrote the manuscript with the assistance and approval of all authors.

INTRODUCTION

Cell growth and proliferation are intimately coordinated with metabolism. Potentially distinct differences in metabolism between normal and cancerous cells has sparked a renewed interest in targeting metabolic enzymes as an approach to the discovery of new anti-cancer therapeutics. The metabolic strategies utilized by cancer cells to enhance proliferative capacity under nutrient-limiting conditions remain controversial and poorly understood. It has thus been unclear as to which aspects of cell metabolism might represent a realistic, targetable vulnerability of tumors relative to normal cells and tissues.

We recently found that prototrophic yeast cells monitor intracellular levels of acetyl-CoA in order to commit to a new round of cell division (Cai et al., 2011; Shi and Tu, 2013). Acetyl-CoA is a key intermediate of carbon sources which not only fuels ATP production via the TCA cycle, but also functions as an essential building block for the synthesis of fatty acids and sterols. When yeast cells commit to cell division, they significantly enhance the production of acetyl-CoA. Elevated levels of acetyl-CoA induce acetylation of histones on a set of more than 1,000 genes critical for cell growth (Cai et al., 2011). This battery of "growth genes" includes virtually all genes important for ribosome biogenesis, protein translation, and amino acid biosynthesis. Transcription of the key G1 cyclin (*CLN3*) that gates entry of yeast cells into the cell division cycle is also dependent upon the ability of cells to substantially enhance the intracellular abundance of acetyl-CoA (Shi and Tu, 2013). Thus, in budding yeast, acetyl-CoA is a sentinel metabolite that regulates transcription of growth genes via epigenetic modification of chromatin (Cai and Tu, 2011; Kaelin and McKnight, 2013).

The strict dependence of yeast cells on acetyl-CoA for cell growth and proliferation prompted us to examine whether acetyl-CoA might also be rate-limiting for mammalian cell growth. In well-fed mammalian cells, the acetyl-CoA used for lipid synthesis and histone acetylation is primarily supplied by mitochondrially-derived citrate (Srere, 1959; Wellen et al., 2009). This metabolite is enzymatically converted into acetyl-CoA via ATP citrate lyase (ACLY) (Srere, 1959; Srere and Lipmann, 1953). Cells grown under the nutrient-unlimited conditions of tissue culture medium also make acetyl-CoA via citrate consumption. By contrast, the nutrient-limiting conditions of tumor growth in animals and humans bring to question what pathways might be primarily utilized for acetyl-CoA production. The phenomenon of aerobic glycolysis famously characterized by Otto Warburg described the truncation of glucose oxidation at pyruvate (Warburg, 1956a, b). Instead of pyruvate being transported into mitochondria for conversion into acetyl-CoA by the pyruvate dehydrogenase complex, many cancer cells are highly glycolytic and preferentially convert pyruvate into lactate. If pyruvate fails to enter the TCA cycle in cancer cells, how is it that sufficient citrate is made for ACLY-mediated production of acetyl-CoA?

Several groups have recently demonstrated the conversion of glutamine into acetyl-CoA via the phenomenon of reductive carboxylation whereby the TCA cycle can be modified to run in reverse (Le et al., 2012; Leonardi et al., 2012; Metallo et al., 2012; Mullen et al., 2012; Wise et al., 2011). Whereas evidence supportive of reductive carboxylation has been obtained in studies of cancer cells grown in tissue culture, *in vivo* studies of primary human

glioblastomas (GBMs) to date have revealed little or no catabolism of glutamine (Marin-Valencia et al., 2012). These GBMs instead exhibit substantive mitochondrial oxidation and a net synthesis of glutamine from glucose. Thus, the ability of glutamine to function as a source of acetyl-CoA in native tumors remains unclear.

These perplexing observations led us to consider alternative sources of acetyl-CoA for tumors in which, as a result of highly glycolytic or hypoxic metabolic environments, glucose-derived pyruvate is preferentially shunted towards lactate instead of acetyl-CoA. Budding yeast lack ATP citrate lyase and instead rely on a family of enzymes called acetyl-CoA synthetases (De Virgilio et al., 1992; Takahashi et al., 2006; van den Berg et al., 1996). Acetyl-CoA synthetases catalyze the synthesis of acetyl-CoA from acetate and CoA in an ATP-dependent reaction (Berg, 1956; Jones et al., 1953; Lipmann and Tuttle, 1945). We hypothesized that the mammalian versions of these acetyl-CoA synthetase enzymes might help cancer cells produce acetyl-CoA from acetate under the challenging growth conditions of solid tumors. Consistent with this idea, acetate could rescue histone acetylation in cell lines in which ACLY was knocked down, although the physiological relevance of acetate in mammalian cells was questioned (Wellen et al., 2009). However, a role for acetate in fueling tumor growth is supported by PET imaging studies using [^{11}C]acetate wherein numerous clinical studies have documented avid acetate uptake in prostate, lung, liver and brain cancers (Ho et al., 2003; Nomori et al., 2008; Oyama et al., 2002; Tsuchida et al., 2008). Indeed, in certain cases [^{11}C]acetate PET imaging is more accurate and sensitive than [^{18}F]fluorodeoxyglucose (FDG) PET imaging, and some tumors are [^{11}C]acetate-positive yet FDGnegative. These considerations have led to the proposal that acetyl-CoA synthetase enzymes could be important for [^{11}C]acetate uptake and tumor cell survival (Yoshii et al., 2009a; Yoshii et al., 2009b; Yun et al., 2009). In the accompanying manuscript, acetate consumption by human tumors has recently been confirmed by NMR-facilitated [^{13}C]acetate metabolic tracer experiments (related paper in this issue). Here we report evidence that the nucleocytosolic ACSS2 enzyme is of critical importance for mammalian cells to utilize acetate as a source of acetyl-CoA, and that mice lacking this enzyme exhibit a substantial reduction in tumor burden in two genetic models of liver cancer.

RESULTS

ACSS2 is Required for Acetate Uptake and Utilization in Mammalian Cells

The mammalian genome contains genes encoding three different enzymes capable of catalyzing the ATP-dependent synthesis of acetyl-CoA from acetate (Watkins et al., 2007). Two such enzymes, designated ACSS1 and ACSS3, are mitochondrial proteins (Fujino et al., 2001; Perez-Chacon et al., 2009). The third, designated ACSS2, has been reported to be localized to both the cytoplasmic and nuclear compartments of mammalian cells (Ariyannur et al., 2010; Luong et al., 2000). In order to assess the relative contributions of these enzymes for cellular utilization of acetate for either lipid synthesis or histone acetylation, RNAi agents were deployed to selectively silence their respective production. After having observed substantive, RNAi-mediated suppression of ACSS1, ACSS2, and ACSS3 (Figure S1), cells were exposed to ^{14}C-labeled acetate in order to measure incorporation of acetyl units into either lipids or histones. RNAi-mediated suppression of ACSS2 led to a more

significant diminution in both lipid and histone assimilation of radiolabeled acetate than suppression of ACSS1 or ACSS3 (Figures 1A–B).

In order to pursue these observations in a more rigorous manner, mouse embryonic fibroblasts (MEFs) were prepared from embryos of mice bearing inactivating mutations in both alleles of ACSS2 (ACSS2−/−). Littermate embryos heterozygous for the ACSS2 mutation (ACSS2−/+), and wild type littermates (ACSS2+/+), were also used to prepare MEFs (Figure S1). When exposed to [^{14}C]acetate, ACSS2−/− MEFs showed a substantial deficit in label incorporation into both lipids and histones relative to ACSS2+/+ MEFs (Figures 1C–D). Cells heterozygous for ACSS2 (+/−) revealed an intermediate decrement in [^{14}C]acetate uptake.

As a third means of testing the importance of ACSS2 for acetate uptake into mammalian cells, a high-throughput screen was conducted in search of chemical inhibitors of the enzyme. Purified, recombinant human ACSS2 enzyme was screened against roughly 200,000 drug-like chemicals housed within the UTSWMC compound file. The details of this screen are presented in the Experimental Procedures. Among hundreds of primary hits cross-screened for reversibility, dose-responsive potency, and selectivity with respect to inhibition of medium- and long-chain Coenzyme A-dependent acyl-CoA synthetase enzymes, a small molecule quinoxaline having an IC_{50} of ~0.6 μM in biochemical assays, and ~5 μM in its ability to inhibit cellular [^{14}C]acetate uptake into both lipids and histones (Figures 1E–F), emerged as one of the most favorable inhibitors of ACSS2. Moreover, this inhibitor did not reduce the residual acetate uptake observed in ACSS2−/− MEFs (Figure S1). The fact that a selective chemical inhibitor of ACSS2 substantially inhibits acetate incorporation into both lipids and histones further confirms the importance of this enzyme for cellular uptake of acetate.

As a final test of the importance of ACSS2 for acetate uptake, shRNA-mediated attenuation of ACSS2 was tested on four different cancer cell lines, including LL/2, PC3, U2OS and Hep3B (Figure S1). In all four cancer cell lines, attenuation of ACSS2 led to a significant impediment to [^{14}C]acetate uptake into both lipids and histones (Figures 1G–H). The combination of shRNA-mediated mRNA knockdown approaches, studies of MEFs selectively mutated at the ACSS2 locus, and the identification of a selective chemical inhibitor of ACSS2 provide strong evidence that this particular enzyme is primarily responsible for allowing mammalian cells to convert acetate into acetyl-CoA for subsequent metabolic utilization.

Reduced Tumor Formation in ACSS2-Deficient Mice

As a means of testing the contribution of ACSS2 to tumorigenesis, we introduced the ACSS2-null allele into a strain of genetically-engineered mice that develop liver cancer due to expression of a liverspecific, doxycycline (dox)-regulated transgene encoding the SV40 early region (ApoE-rtTA$_{M2}$:TRE2-TAg; herein referred to as TAg). Notably, adult ACSS2-null mice display no overt phenotypic deficits and both sexes are fertile. Cohorts of male and female TAg mice with and without ACSS2 were generated as described in Experimental Procedures and provided with drinking water supplemented with 10 μg/mL doxycycline for 42–45 days. This regimen promotes reproducible and robust multifocal tumor development

in a background of hepatic hyperplasia (Comerford et al., 2012). Post-sacrifice, livers were scored for tumor development using a non-linear tumor-burden scale based on the number and size of visible tumors on the surface of the liver, % liver/body weight, and the relative amount of tumor-free liver as described in detail (Table S2).

After 42–45 days of dox treatment, livers of ACSS2+/+:TAg mice were covered with small to medium-sized tumors reflecting multifocal tumor growth in response to sustained expression of the SV40 large T and small t (LT/st) oncoproteins. 20/21 mice (95%) exhibited tumor burden scores of 8 or greater (Figure 2A). By contrast, only 48% of ACSS2−/−:TAg mice exhibited tumor growth of an equivalent magnitude, with almost half (41%) receiving scores of 6 or lower. The statistical significance in the overall reduction in mean tumor burden score from 9.4 to 6.8 in mice with and without ACSS2 achieved a calculated p-value of 0.0002 (Figure 2A). Given that tumor burdens within the 9–10 range and 6–7 range reflected the presence of 100–200 tumors (too many to accurately count), or 20–50 tumors respectively, these data indicate that ACSS2-deficiency reduces the absolute number of liver tumors by at least 4-fold.

Having shown that loss of ACSS2 correlates with reduced tumor burdens in the TAg liver cancer model, we next asked what impact of loss of ACSS2 might have on the development of tumors driven by c-Myc overexpression and loss of PTEN, both of which are associated with human hepatocarcinogenesis (Kawate et al., 1999; Peng et al., 1993; Yao et al., 1999). In this genetically-engineered mouse model, liver-specific expression of c-Myc (Sandgren et al., 1989), in conjunction with hepatic deletion of the PTEN tumor suppressor ($PTEN^{lox/lox}$) (Lesche et al., 2002), promotes the development of at least two large tumors (>10mm) per liver in a background of hepatomegaly in 90% of mice at 6–7 months of age (Comerford and Hammer, unpublished observations). This second liver cancer model, herein referred to as c-Myc:ΔPTEN, constitutes a more stochastic and clinically relevant model of hepatic tumor development than the SV40 TAg model. Cohorts of male and female c-Myc:ΔPTEN mice with and without ACSS2 were generated as described in Experimental Procedures and sacrificed at 6–7 months of age. Livers were scored for tumor development using a scale that differed from the one used to score the TAg tumors to accommodate the more stochastic pattern of tumor development in these mice (Table S2).

At 6–7 months of age, 20/24 (83%) of ACSS2+/+:cMyc:ΔPTEN mice had livers with at least 10 visible tumors (2–15mm in size), resulting in assignment of tumor burden scores of 7 or greater (Figure 2B). This was in direct contrast to cohorts of age-matched ACSS2−/−:c-Myc:ΔPTEN mice in which only 6/21 mice (29%) had tumor burdens of 7 or greater. Indeed, ACSS2-deficiency not only reduced the mean tumor burden score from 7.8 to 4.7 ($p < 0.0001$), but inhibited tumor growth to such an extent that 71% of ACSS2-deficient mice had livers with fewer than 10 small tumors, or no tumors at all (Figure 2B).

Immunohistochemical Studies of ACSS2 Expression in Hepatocellular Tumors in Mice

Our results showing that the loss of ACSS2 reduced liver tumor development in two different mouse models suggested that a subset of tumors might be dependent on ACSS2 for growth and therefore express high levels of ACSS2. To determine if this were the case, we surveyed the distribution of ACSS2 expression in normal mouse liver and in tumor-bearing

livers from both cancer models by performing IHC with an ACSS2-specific antibody. In livers of WT mice, ACSS2 was highly expressed in the cytoplasm and nucleus of hepatocytes in periportal zones 1 and 2 with virtually no expression evident in centrilobular zone 3 or in bile ducts (Figure 3A). Moreover, livers of ACSS2-null mice were devoid of any immunoreactivity indicating absolute specificity of the antibody for ACSS2 and lack of any cross-reactivity with ACSS1, ACSS3, or other acyl-CoA synthetase enzymes (Figure 3A).

The expression of ACSS2 in tumors from the TAg and c-Myc:ΔPTEN mice showed significant heterogeneity both between and within individual tumors (Figure 3A). Approximately 56% of TAg and 75% of c-Myc:ΔPTEN tumors contained ACSS2-positive cells (Table S3), while the remainder contained none. Given that ACSS2-positive tumors varied with respect to the proportion of ACSS2-expressing cells, a scoring method was devised to classify tumors as $ACSS2^{HIGH,\ MED\ or\ LOW}$ according to the percentage of ACSS2-positive cells within each tumor (see Experimental Procedures). Using this method, we determined that approximately half of the ACSS2-positive tumors in each tumor model (53% of TAg and 58% of c-Myc:ΔPTEN tumors) were either $ACSS2^{HIGH}$ or $ACSS2^{MED}$, while the remainder were $ACSS2^{LOW}$ (Table S3). In several tumors, focal areas of prominent nuclear ACSS2 staining were seen, suggesting that enhanced translocation of ACSS2 from the cytoplasm to the nucleus might be associated with tumorigenesis, although this was not a universal finding. Importantly, evaluation of ACSS2 expression in c-Myc:ΔPTEN livers where tumors were juxtaposed to areas of liver in which normal hepatic zonation had been maintained, showed that the level of ACSS2 expressed in $ACSS2^{HIGH}$ tumors was comparable to that found in normal periportal hepatocytes, suggesting that ACSS2 expression was maintained, rather than induced, in a subset of tumors, and was lost in others. As expected, tumor-bearing livers from ACSS2-deficient TAg or c-Myc:ΔPTEN mice were devoid of any immunoreactivity.

Having shown that the loss of ACSS2 reduced tumor incidence in both liver cancer models, we next determined if ACSS2-deficiency altered the tumor spectrum. Comparative histological analysis of H&E stained sections of tumor-bearing livers of ACSS2+/+ and ACSS2−/− TAg and c-Myc:ΔPTEN mice showed that ACSS2-deficiency increased the proportion of well-differentiated HCCs at the expense of moderately-poorly differentiated HCCs and other tumor types in both models (Figure S2), suggesting that ACSS2 drives the emergence of more aggressive hepatic tumors in the mouse.

Immunohistochemical Studies of ACSS2 Expression in Human Tumors

Clinical imaging studies have observed avid [^{11}C]acetate uptake in a wide spectrum of human cancers, including prostate, liver, lung and brain tumors (Ho et al., 2003; Nomori et al., 2008; Oyama et al., 2002; Tsuchida et al., 2008). It has been proposed that acetate uptake in these tumors might reflect expression of the acetyl-CoA synthetase enzymes, including ACSS2 (Yoshii et al., 2009b; Yun et al., 2009). In normal adult mice, ACSS2 mRNA is most abundantly expressed in liver and kidney, with lower levels present in the heart, brain, and testis (Luong et al., 2000). We next surveyed the extent of ACSS2 protein expression in a variety of human tumor samples by immunohistochemical staining of

commercially available tumor tissue microarrays. Significant ACSS2 expression was observed in a substantial number of human breast, ovarian, and lung tumor samples (Figure 3B). Normal, non-cancerous samples of the tissues of origin exhibited little to no ACSS2 protein at all.

We then surveyed ACSS2 expression in a well-annotated set of human triple negative breast cancers (Figures 4A and S3). Immunohistochemical analysis was available for 154 cases after discounting loss of cores due to sectioning and IHC processing. Expression was stratified into three categories for association with overall survival. High expression of ACSS2 (H score 120–300) was associated with shorter overall survival compared to ACSS2-negative cases ($p=0.03$) (Figure 4B). However, the observed correlation between ACSS2 expression and decreased survival does not necessarily imply dependency. Expression of ACSS2 was observed predominantly in the cytoplasm with some cases exhibiting significant nuclear staining. Taken together, these observations strongly suggest that ACSS2 is expressed to a significant extent in particular tumor types, including triple negative breast cancers.

[^{11}C]Acetate PET Imaging of Hepatocellular Tumors in Mice

To directly test whether [^{11}C]acetate uptake correlated with ACSS2 expression in the mouse models of liver cancer, we performed [^{11}C]acetate PET imaging of tumors developing in the c-Myc:ΔPTEN and TAg mice. We observed the expected biodistribution for [^{11}C]acetate in WT mice, with modest uptake in normal liver. In contrast, mice bearing liver tumors exhibited greater uptake in the liver, with focal regions of significantly greater [^{11}C]acetate uptake (Figures 5A–D). Tracer pharmacokinetics appeared to reach a state of equilibrium between 25 and 40 min post-radiotracer administration, as depicted in the time-activity curves (TAC) (Figure 5E). During this time interval, radiotracer concentration within the tumor region-of-interest (ROI) was nearly 3 times greater in tumors arising in the c-Myc:ΔPTEN mice compared to uptake in normal liver. Presence of tumor was confirmed histologically and exhibited significant staining of ACSS2 (Figure 5F). The imaged tumor in the TAg mouse exhibited only modestly higher [^{11}C]acetate uptake which correlated with lower expression of ACSS2. Moreover, several [^{11}C]acetate-negative tumors arising in the TAg mice showed virtually no expression of ACSS2 protein at all, and [^{11}C]acetate uptake was lower in liver from an ACSS2−/− mouse compared to WT (Figure S4). Collectively, these observations demonstrate a strong correlation between [^{11}C]acetate uptake and ACSS2 expression.

DISCUSSION

Here we describe experiments indicating that certain tumors may have evolved a dependency on acetate as a carbon source for the production of acetyl-CoA. This conclusion is, for many reasons, perplexing. Unlike the low millimolar levels of blood glucose, which is a considerably more energetic carbon source than acetate, blood level measurements for acetate are estimated at ~20–50 μM (Psychogios et al., 2011; Tollinger et al., 1979). How could an energy-diminished metabolite, relative to glucose, feed tumors when its abundance in blood is two orders of magnitude lower than glucose? Before offering possible

explanations to this conundrum, it may be of value to compare the evolution of human tumors to the work of Richard Lenski and colleagues on bacterial evolution (Blount et al., 2012). By continually growing a dozen separate cultures of *E. coli* for upwards of 25 years, Lenski and colleagues have evolved derivatives that out-compete the starting bacterial cells via enhanced cell growth rates in the range of 70%. Two of Lenski's twelve cultures were found to have achieved enhanced growth via the induction of pathways facilitating the catabolism of citrate. We offer the hypothesis that during the evolution of certain tumors, a Lenski-like adaptation may have taken place – not to citrate dependence, but to acetate dependence.

In support of this idea, we offer the following considerations. [^{11}C]acetate PET imaging studies have shown that many human cancers avidly take up acetate, and confirmatory [^{13}C]acetate NMR tracer studies also reveal selective acetate uptake in human tumors (related paper in this issue). Moreover, substantive ACSS2 immunohistochemical staining of both hepatic tumors in mice and numerous tumors from humans reveals strong expression of the enzyme (Figures 3–4). Indeed, we observe a strong correlation between ACSS2 expression and uptake of [^{11}C]acetate into liver tumors in mice (Figure 5). As shown here, for mammalian cells ACSS2 is the most important member of this enzyme family for uptake of acetate and its conversion into lipids and acetylated histones (Figure 1). Lastly, animals bearing targeted mutations in both alleles of the ACSS2 gene show a substantially diminished tumor burden in two genetic models of cancer (Figure 2). We simplistically conclude that certain tumors are able to avidly capture acetate to help fuel their growth and survival (Figure 6). If normal cells and tissues are far less competent in acquiring and retaining acetate, then tumors may be able to survive and grow by avid consumption of this sub-optimal hydrocarbon fuel.

Studies of prototrophic yeast grown continuously in a chemostat offer a framework for thinking about how mammalian tissues might share acetate. When grown at high density under continuous, glucose-limitation conditions, yeast cells enter into a robust metabolic cycle in which a population of yeast cells synchronously oscillates (Tu et al., 2005). During glycolytic growth, cells consume glucose and ferment the carbon source all the way to ethanol. By contrast, during respiratory growth, ethanol is retrieved as a carbon source via its sequential anabolic conversion into acetaldehyde, acetate, and acetyl-CoA. Indeed, the periodic secretion and uptake of ethanol and acetate can be observed as a function of the yeast metabolic cycle (Tu et al., 2005), revealing that these simple products of glycolysis can be secreted and then shared amongst sub-populations of the community.

We offer the speculative idea that acetate is liberally moved in and out of mammalian cells and tissues in a dynamic fashion. As acetate is not typically thought to be a physiologically significant carbon source in mammals, what are the possible sources of acetate? The half-life of acetyl modifications on histones has been measured to be on the order of only ~2–3 minutes as a result of the opposing actions of histone acetyltransferase and deacetylase enzymes (Jackson et al., 1975; Waterborg, 2002). Histone proteins are amongst the most abundant in cells and several dozen sites within each histone octamer are subject to modification by acetylation (Shahbazian and Grunstein, 2007). Considering the extremely short half-life of acetylation modifications, substantial quantities of acetate could be

continuously released from histone tails simply as a result of deacetylation. Moreover, if certain tumor cells liberally secrete lactate via the truncation in glycolysis discovered by Otto Warburg, neighboring normal cells could convert lactate back into pyruvate, thereby yielding a possible source of acetyl-CoA. Acetyl-CoA hydrolase or thioesterase enzymes could re-balance metabolism such that acetate could be liberated from normal cells as a hydrocarbon source for rogue consumption by tumor cells. In other words, if a tumor cell were hard-wired to exist in an acetate-capturing or fixing state, it might significantly out-compete the rest of the human body in its ability to feed upon a sub-optimal carbon source present at relatively low concentrations.

At the cost of a single ATP, one acetate molecule can be retrieved to produce acetyl-CoA for use in the synthesis of fatty acids or sterols, for the acetylation of histones, or for further oxidation via the TCA cycle to generate an additional ~12 units of ATP (Figure 6). Acetate can also be used for the synthesis of the amino acid glutamate (related paper in this issue). Unlike yeast, mammals lack a glyoxylate cycle and therefore cannot utilize acetate for the synthesis of glucose. Nonetheless, the ability to recoup acetate for any of these other purposes stands to promote tumor cell growth or survivability in the face of nutritionally challenging or hypoxic microenvironments. In contrast, acetate might be irrelevant for nutritionally-replete cells or tissues. Given ample supplies of glucose, coupled with the ability to convert glucose into acetyl-CoA via citrate spilling out of mitochondria, normal cells or tissues might actually represent net producers of acetate, rather than net consumers.

Were it indeed the case that certain tumors acquire, via expression of ACSS2, a strict dependency on acetate for their growth or survival, then selective inhibitors of this non-essential enzyme might represent an unusually ripe opportunity for the development of new anti-cancer therapeutics. By screening a library of 200,000 drug-like chemicals, we have discovered compounds that are capable of selectively inhibiting ACSS2 relative to other acyl-CoA synthetase enzymes that ligate Coenzyme A onto medium or long chain fatty acids. It is hoped that these chemical inhibitors of ACSS2 can be optimized for potency, selectivity and pharmacological properties. If the normal human cells and tissues are not heavily reliant on the activity of the ACSS2 enzyme, it is possible that such agents might inhibit the growth of ACSS2-expressing tumors with a favorable therapeutic window.

EXPERIMENTAL PROCEDURES

Construction of Stable Knockdown Cell Lines

Cells were seeded in 60 mm dishes to 30% confluence the day before infection. 1 mL fresh medium and 1 mL retrovirus (treated with 8 μg/mL polyberen) carrying shRNA against ACSS1, ACSS2, ACSS3 or REN (Renilla luciferase) as control were added during virus infection. Puromycin was added at 2 μg/mL to the medium for selection at 48–60 h after infection. Medium was replaced with fresh medium supplemented with puromycin every 1 or 2 days. Cells were split as they became confluent. Puromycin was maintained in the medium for selection up to 10 days. Sequences of shRNA used:

shREN: AGGAATTATAATGCTTATCTA

shACSS1: CCAGTTAAATGTCTCTGTCAA

shACSS2: CAGGATTGATGACATGCTCAA

shACSS3: GCCGTTGATCGTCATATTGAA

[^{14}C]Acetate Incorporation into Lipid Fractions

Cells were grown in 12-well plates to 70–80% confluence. Cells were treated with 1 μCi/mL sodium [1,2-^{14}C]acetate (PerkinElmer) for 6 h. After two washes with ice-cold PBS, cells were lysed with 0.6 mL MeOH solution (MeOH:H_2O=2.5:1). 0.4 mL $CHCl_3$ was added to lysate and mixed by vortexing for 30 s. Lysates were then centrifuged for 5 min at 1,000 rpm for phase separation. The lipid soluble fraction was collected as the lower layer. Fractions were counted for radioactivity.

[^{14}C]Acetate Incorporation into Histones

Cells were grown in 6-well plates to 70–80% confluence. Cells were treated with 1 μCi/mL [^{14}C]acetate for 6 h. After two washes with ice-cold PBS, cells were lysed in hypotonic buffer (10 mM Tris-Cl pH 8.0, 1 mM KCl, 1.5 mM $MgCl_2$, 1 mM DTT) with protease inhibitors, and then subjected to one freeze/thaw cycle at −20°C. Lysates were centrifuged at 4°C 10,000g for 10 min. Supernatants were discarded, the pellets were re-suspended in 400 μL 0.4 N H_2SO_4, and vortexed until pellets were dissolved. The lysates were rotated at 4°C overnight and then centrifuged at 4°C 16,000g for 10 min. Supernatants were taken and counted for radioactivity.

Scoring of Tumor Burdens

Tumor burden scores were assigned on the basis of the number and size of tumors, the magnitude of hepatic hyperplasia and the amount of tumor-free liver remaining after 42–45 days of dox treatment (TAg model) or at 6–7 months of age (c-Myc:ΔPTEN model). A detailed description of criteria used to assign tumor burden scores in each model is provided in Table S2. Scores were assigned by SAC or REH.

Scoring of ACSS2 Expression in Tumors

Tumor scoring for ACSS2 expression was conducted by performing IHC with the ACSS2-specific antibody on formalin fixed paraffin-embedded sections of liver from TAg mice provided with dox for 42–45 days and from 6–7 month old c-Myc:ΔPTEN mice. Each slide contained sections cut from a block containing a minimum of 6 randomly selected pieces of liver collected at the time of sacrifice. A total of 80 tumors from the TAg mice and 32 from the c-Myc:ΔPTEN mice were surveyed. The average number of TAginduced tumors surveyed/slide was 20 (range; 15–25) while the average number of c-Myc:ΔPTEN-driven tumors/slide was 8 (range; 7–10). Tumors were scored on the basis of the number of ACSS2-positive cells within each tumor: Tumors were designated ACSS2^{HIGH}, ACSS2^{MED}, or ACSS2^{LOW} if they contained > 60%, 30–60% or < 30% ACSS2-positive cells respectively. Tumors that did not contain any visible ACSS2-positive cells were designated ACSS2^{NEG}. Tumor-specific expression of ACSS2 was independently scored by SAC and ZH.

Human Triple Negative Breast Cancer Tissue Microarray

Tissue microarray with 168 triple negative breast carcinoma (TNBC) cases was employed to evaluate ACSS2 protein expression by immunohistochemistry. Tissues present on the array were obtained with Institutional Review Board approval. TNBC clinical designation was defined as the absence of staining for estrogen receptor, progesterone receptor, and *HER2/neu*. Clinical and pathologic variables were determined following well-established criteria. All invasive carcinomas were graded according to the method described by Elston and Ellis (Elston and Ellis, 1991). The tissue microarrays (TMA) were constructed as previously described using a tissue arrayer (Beecher Instruments, Silver Spring, MD). Two tissue cores (0.6 mm diameter) were sampled from each block and transferred to the recipient TMA block.

All ACSS2-stained slides were scanned using the ScanScope System (Aperio Technologies, Inc., Vista, CA, USA) and viewed using ImageScope software (Aperio). Pathologist with subspecialty training in breast pathology (AKW) assured that areas selected for automated image analysis represented tumor. Staining intensity was graded with: none as 0, weak as 1+, moderate as 2+, and marked as 3+. The percentage of stained tumor cells was recorded. H-score was calculated as previously described using the following formula (1 × % of weak staining) + (2 × % moderate staining) + (3 × % marked staining). Duplicates of cores were scored separately and the highest-yielding H-score among the three constructs was selected.

Data and associations were assessed using the R-statistical package. Kaplan–Meier survival curves were used to estimate overall survival, which was defined as the time from date of surgery to date death from TNBC or to the last follow-up date for censored cases. The log-rank test was performed to compare survival between groups. A *P*-value of <0.05 was considered significant.

High-Throughput Screen to Identify inhibitors of Human ACSS2

Human ACSS2 enzyme was expressed in insect cells using the Invitrogen Bac to Bac expression system. Acetyl-CoA (C4780) and pyrophosphatase (I1643) were purchased from Sigma. CellTiter-Glo® was purchased from Promega. EnzChek® Pyrophosphate Assay Kit (E6645), which includes purine nucleotide phosphorylase (PNP) and MESG, was purchased from Life Technologies.

ACSS2 converts ATP, acetate, CoA into AMP, pyrophosphate, and acetyl-CoA. In our assay, the reaction was monitored by the disappearance of ATP using a luciferase-based CellTiter-Glo® reagent. The screen was carried out using 384-well plates. A typical reaction mixture contained 0.1 mM CoA, 0.02 mM ATP, 10 mM DTT, 0.1 unit/mL pyrophosphatase, 1 μg/mL ACSS2, 0.1 mg/mL BSA, 150 mM NaCl, 1 mM $MgCl_2$, and 50 mM Hepes, pH 7.5. The reaction was initiated by the addition of 5 μL of 25 mM sodium acetate to each well containing 20 μL reaction mixture. The plates were then spun for 1 minute at 1,500 g and incubated at 37°C. When the reaction reached 70% completion, which typically occurred after 2.5 to 5 hours, 25 μL CellTiter-Glo reagent was added to each well. The plates were shaken for 2 min and luminescence was read on a Perkin Elmer Envision plate reader. The presence of an inhibitor slowed down the consumption of ATP and was revealed by high

luminescence reading on the plate reader. We identified 1152 hits in the primary screen of 220K compounds in our chemical library at UTSWMC. By removing redundant hits in the large structure groups, we cherry-picked 926 hits for further confirmation using the same assay but carried out in triplicate. We were able to confirm 118 of the 926 hits. To test the specificity of the inhibitors, we carried out a counter-screen against ACSF2 (medium chain fatty acid-CoA synthetase) and ACSL5 (long chain fatty acid-CoA synthetase). We were able to identify 62 compounds as specific inhibitors against ACSS2 based on their non-activity against ACSF2 and ACSL5. One of these most potent and specific inhibitors, N-(2,3-di-2-thienyl-6-quinoxalinyl)-N'-(2-methoxyethyl)urea was purchased from ChemBridge (San Diego, CA) and re-tested (Figures 1E–F).

Measurement of IC_{50} of Inhibitors

The measurement of initial rate is ideally carried out when the reaction extent is less than 15%. The variation in the luciferase assay used in the HTS screen is typically around 10%. For this reason, we adopted a different assay for the measurement of reaction rate in the determination of IC_{50} of ACSS2 inhibitors. Instead of monitoring the consumption of ATP, we measured generation of pyrophosphate in a coupled enzymatic assay. The reaction mixture contained pyrophosphatase, which converts pyrophosphate to phosphate, and purine nucleotide phosphorylase (PNP), which couples phosphate with a nucleotide analog (MESG), resulting in a compound that absorbs light at 360 nm. A typical reaction mixture includes 50 μM CoA, 100 μM ATP, 5 mM sodium acetate, 0.2 mM MESG, 0.2% BSA, 20 nM ACSS2, 0.4 μM PNP, 1 unit/mL of yeast pyrophosphatase, 1 mM $MgCl_2$, 150 mM NaCl, and 50 mM HEPES, pH 7.5. The reaction rates were computed by the increase of absorption at 360 nm for a range of inhibitor concentrations. Curve-fitting (rate vs. inhibitor concentration) in PRISM yielded IC_{50}.

Construction of ACSS2 KO mice, mouse breeding and genotyping procedures, isolation of MEFs, and [^{11}C]acetate PET methods are described in Supplemental Experimental Procedures

Supplementary Material

Refer to Web version on PubMed Central for supplementary material.

ACKNOWLEDGMENTS

We thank B. Posner and the staff of the UTSWMC High-Throughput Screening Core Facility for assistance with the ACSS2 inhibitor screen, V. Vemireddy, E. Maher, R. Bachoo, S. Altschuler, L. Wu for use of slide scanners, and E. Maher, R. Bachoo, D. Nijhawan for helpful discussions. This work was supported by a Damon Runyon-Rachleff Innovation Award, Packard Fellowship, and a CPRIT High-Risk/High-Impact grant to BPT, R01CA185169 to BPT and SLM, unrestricted funds provided to SLM by an anonymous donor, and Excellence in Education funds (EEF) from UTSWMC to REH. SLM is the founder and Chairman of the Scientific Advisory Board, XD is an employee, BPT, SAC, REH are consultants, and SLM, BPT, SAC, XD, REH, LC are shareholders of Peloton Therapeutics, Inc.

REFERENCES

Ariyannur PS, Moffett JR, Madhavarao CN, Arun P, Vishnu N, Jacobowitz DM, Hallows WC, Denu JM, Namboodiri AM. Nuclear-cytoplasmic localization of acetyl coenzyme a synthetase-1 in the rat brain. The Journal of comparative neurology. 2010; 518:2952–2977. [PubMed: 20533355]

Berg P. Acyl adenylates; an enzymatic mechanism of acetate activation. J Biol Chem. 1956; 222:991–1013. [PubMed: 13367067]

Blount ZD, Barrick JE, Davidson CJ, Lenski RE. Genomic analysis of a key innovation in an experimental Escherichia coli population. Nature. 2012; 489:513–518. [PubMed: 22992527]

Cai L, Sutter BM, Li B, Tu BP. Acetyl-CoA Induces Cell Growth and Proliferation by Promoting the Acetylation of Histones at Growth Genes. Mol Cell. 2011; 42:426–437. [PubMed: 21596309]

Cai L, Tu BP. On Acetyl-CoA as a Gauge of Cellular Metabolic State. Cold Spring Harb Symp Quant Biol. 2011; 76:195–202. [PubMed: 21900151]

Comerford SA, Schultz N, Hinnant EA, Klapproth S, Hammer RE. Comparative analysis of SV40 17kT and LT function in vivo demonstrates that LT's C-terminus re-programs hepatic gene expression and is necessary for tumorigenesis in the liver. Oncogenesis. 2012; 1:e28. [PubMed: 23552841]

De Virgilio C, Burckert N, Barth G, Neuhaus JM, Boller T, Wiemken A. Cloning and disruption of a gene required for growth on acetate but not on ethanol: the acetyl-coenzyme A synthetase gene of Saccharomyces cerevisiae. Yeast. 1992; 8:1043–1051. [PubMed: 1363452]

Elston CW, Ellis IO. Pathological prognostic factors in breast cancer. I. The value of histological grade in breast cancer: experience from a large study with long-term follow-up. Histopathology. 1991; 19:403–410. [PubMed: 1757079]

Fujino T, Kondo J, Ishikawa M, Morikawa K, Yamamoto TT. Acetyl-CoA synthetase 2, a mitochondrial matrix enzyme involved in the oxidation of acetate. J Biol Chem. 2001; 276:11420–11426. [PubMed: 11150295]

Ho CL, Yu SC, Yeung DW. 11C-acetate PET imaging in hepatocellular carcinoma and other liver masses. J Nucl Med. 2003; 44:213–221. [PubMed: 12571212]

Jackson V, Shires A, Chalkley R, Granner DK. Studies on highly metabolically active acetylation and phosphorylation of histones. J Biol Chem. 1975; 250:4856–4863. [PubMed: 168194]

Jones ME, Lipmann F, Hilz H, Lynen F. On the enzymatic mechanism of Coenzyme A acetylation with adenosine triphosphate and acetate. J Am Chem Soc. 1953; 75:3285–3286.

Kaelin WG Jr, McKnight SL. Influence of metabolism on epigenetics and disease. Cell. 2013; 153:56–69. [PubMed: 23540690]

Kawate S, Fukusato T, Ohwada S, Watanuki A, Morishita Y. Amplification of c-myc in hepatocellular carcinoma: correlation with clinicopathologic features, proliferative activity and p53 overexpression. Oncology. 1999; 57:157–163. [PubMed: 10461064]

Le A, Lane AN, Hamaker M, Bose S, Gouw A, Barbi J, Tsukamoto T, Rojas CJ, Slusher BS, Zhang H, et al. Glucose-independent glutamine metabolism via TCA cycling for proliferation and survival in B cells. Cell Metab. 2012; 15:110–121. [PubMed: 22225880]

Leonardi R, Subramanian C, Jackowski S, Rock CO. Cancer-associated isocitrate dehydrogenase mutations inactivate NADPH-dependent reductive carboxylation. J Biol Chem. 2012; 287:14615–14620. [PubMed: 22442146]

Lesche R, Groszer M, Gao J, Wang Y, Messing A, Sun H, Liu X, Wu H. Cre/loxP-mediated inactivation of the murine Pten tumor suppressor gene. Genesis. 2002; 32:148–149. [PubMed: 11857804]

Lipmann F, Tuttle LC. The detection of activated carboxyl groups with hydroxylamine as interceptor. J Biol Chem. 1945; 161:415. [PubMed: 21005751]

Luong A, Hannah VC, Brown MS, Goldstein JL. Molecular characterization of human acetyl-CoA synthetase, an enzyme regulated by sterol regulatory element-binding proteins. J Biol Chem. 2000; 275:26458–26466. [PubMed: 10843999]

Marin-Valencia I, Yang C, Mashimo T, Cho S, Baek H, Yang XL, Rajagopalan KN, Maddie M, Vemireddy V, Zhao Z, et al. Analysis of tumor metabolism reveals mitochondrial glucose

oxidation in genetically diverse human glioblastomas in the mouse brain in vivo. Cell Metab. 2012; 15:827–837. [PubMed: 22682223]

Metallo CM, Gameiro PA, Bell EL, Mattaini KR, Yang J, Hiller K, Jewell CM, Johnson ZR, Irvine DJ, Guarente L, et al. Reductive glutamine metabolism by IDH1 mediates lipogenesis under hypoxia. Nature. 2012; 481:380–384. [PubMed: 22101433]

Mullen AR, Wheaton WW, Jin ES, Chen PH, Sullivan LB, Cheng T, Yang Y, Linehan WM, Chandel NS, DeBerardinis RJ. Reductive carboxylation supports growth in tumour cells with defective mitochondria. Nature. 2012; 481:385–388. [PubMed: 22101431]

Nomori H, Shibata H, Uno K, Iyama K, Honda Y, Nakashima R, Sakaguchi K, Goya T, Takanami I, Koizumi K, et al. 11C-Acetate can be used in place of 18F-fluorodeoxyglucose for positron emission tomography imaging of non-small cell lung cancer with higher sensitivity for well-differentiated adenocarcinoma. Journal of thoracic oncology : official publication of the International Association for the Study of Lung Cancer. 2008; 3:1427–1432.

Oyama N, Akino H, Kanamaru H, Suzuki Y, Muramoto S, Yonekura Y, Sadato N, Yamamoto K, Okada K. 11C-acetate PET imaging of prostate cancer. J Nucl Med. 2002; 43:181–186. [PubMed: 11850482]

Peng SY, Lai PL, Hsu HC. Amplification of the c-myc gene in human hepatocellular carcinoma: biologic significance. J Formos Med Assoc. 1993; 92:866–870. [PubMed: 7511953]

Perez-Chacon G, Astudillo AM, Balgoma D, Balboa MA, Balsinde J. Control of free arachidonic acid levels by phospholipases A2 and lysophospholipid acyltransferases. Biochim Biophys Acta. 2009; 1791:1103–1113. [PubMed: 19715771]

Psychogios N, Hau DD, Peng J, Guo AC, Mandal R, Bouatra S, Sinelnikov I, Krishnamurthy R, Eisner R, Gautam B, et al. The human serum metabolome. PLoS One. 2011; 6:e16957. [PubMed: 21359215]

Sandgren EP, Quaife CJ, Pinkert CA, Palmiter RD, Brinster RL. Oncogene-induced liver neoplasia in transgenic mice. Oncogene. 1989; 4:715–724. [PubMed: 2543942]

Shahbazian MD, Grunstein M. Functions of site-specific histone acetylation and deacetylation. Annu Rev Biochem. 2007; 76:75–100. [PubMed: 17362198]

Shi L, Tu BP. Acetyl-CoA induces transcription of the key G1 cyclin CLN3 to promote entry into the cell division cycle in Saccharomyces cerevisiae. Proc Natl Acad Sci U S A. 2013; 110:7318–7323. [PubMed: 23589851]

Srere PA. The citrate cleavage enzyme. I. Distribution and purification. J Biol Chem. 1959; 234:2544–2547. [PubMed: 13833535]

Srere PA, Lipmann F. An enzymatic reaction between citrate, adenosine triphosphate and Coenzyme A. J Am Chem Soc. 1953; 75:4874.

Takahashi H, McCaffery JM, Irizarry RA, Boeke JD. Nucleocytosolic acetyl-coenzyme a synthetase is required for histone acetylation and global transcription. Mol Cell. 2006; 23:207–217. [PubMed: 16857587]

Tollinger CD, Vreman HJ, Weiner MW. Measurement of acetate in human blood by gas chromatography: effects of sample preparation, feeding, and various diseases. Clinical chemistry. 1979; 25:1787–1790. [PubMed: 476928]

Tsuchida T, Takeuchi H, Okazawa H, Tsujikawa T, Fujibayashi Y. Grading of brain glioma with 1-11C-acetate PET: comparison with 18F-FDG PET. Nucl Med Biol. 2008; 35:171–176. [PubMed: 18312826]

Tu BP, Kudlicki A, Rowicka M, McKnight SL. Logic of the yeast metabolic cycle: temporal compartmentalization of cellular processes. Science. 2005; 310:1152–1158. [PubMed: 16254148]

van den Berg MA, de Jong-Gubbels P, Kortland CJ, van Dijken JP, Pronk JT, Steensma HY. The two acetyl-coenzyme A synthetases of Saccharomyces cerevisiae differ with respect to kinetic properties and transcriptional regulation. J Biol Chem. 1996; 271:28953–28959. [PubMed: 8910545]

Warburg O. On respiratory impairment in cancer cells. Science. 1956a; 124:269–270. [PubMed: 13351639]

Warburg O. On the origin of cancer cells. Science. 1956b; 123:309–314. [PubMed: 13298683]

Waterborg JH. Dynamics of histone acetylation in vivo. A function for acetylation turnover? Biochem Cell Biol. 2002; 80:363–378. [PubMed: 12123289]

Watkins PA, Maiguel D, Jia Z, Pevsner J. Evidence for 26 distinct acyl-coenzyme A synthetase genes in the human genome. J Lipid Res. 2007; 48:2736–2750. [PubMed: 17762044]

Wellen KE, Hatzivassiliou G, Sachdeva UM, Bui TV, Cross JR, Thompson CB. ATP-citrate lyase links cellular metabolism to histone acetylation. Science. 2009; 324:1076–1080. [PubMed: 19461003]

Wise DR, Ward PS, Shay JE, Cross JR, Gruber JJ, Sachdeva UM, Platt JM, DeMatteo RG, Simon MC, Thompson CB. Hypoxia promotes isocitrate dehydrogenase-dependent carboxylation of alpha-ketoglutarate to citrate to support cell growth and viability. Proc Natl Acad Sci U S A. 2011; 108:19611–19616. [PubMed: 22106302]

Yao YJ, Ping XL, Zhang H, Chen FF, Lee PK, Ahsan H, Chen CJ, Lee PH, Peacocke M, Santella RM, et al. PTEN/MMAC1 mutations in hepatocellular carcinomas. Oncogene. 1999; 18:3181–3185. [PubMed: 10340391]

Yoshii Y, Furukawa T, Yoshii H, Mori T, Kiyono Y, Waki A, Kobayashi M, Tsujikawa T, Kudo T, Okazawa H, et al. Cytosolic acetyl-CoA synthetase affected tumor cell survival under hypoxia: the possible function in tumor acetyl-CoA/acetate metabolism. Cancer Sci. 2009a; 100:821–827. [PubMed: 19445015]

Yoshii Y, Waki A, Furukawa T, Kiyono Y, Mori T, Yoshii H, Kudo T, Okazawa H, Welch MJ, Fujibayashi Y. Tumor uptake of radiolabeled acetate reflects the expression of cytosolic acetyl-CoA synthetase: implications for the mechanism of acetate PET. Nucl Med Biol. 2009b; 36:771–777. [PubMed: 19720289]

Yun M, Bang SH, Kim JW, Park JY, Kim KS, Lee JD. The importance of acetyl coenzyme A synthetase for 11C-acetate uptake and cell survival in hepatocellular carcinoma. J Nucl Med. 2009; 50:1222–1228. [PubMed: 19617323]

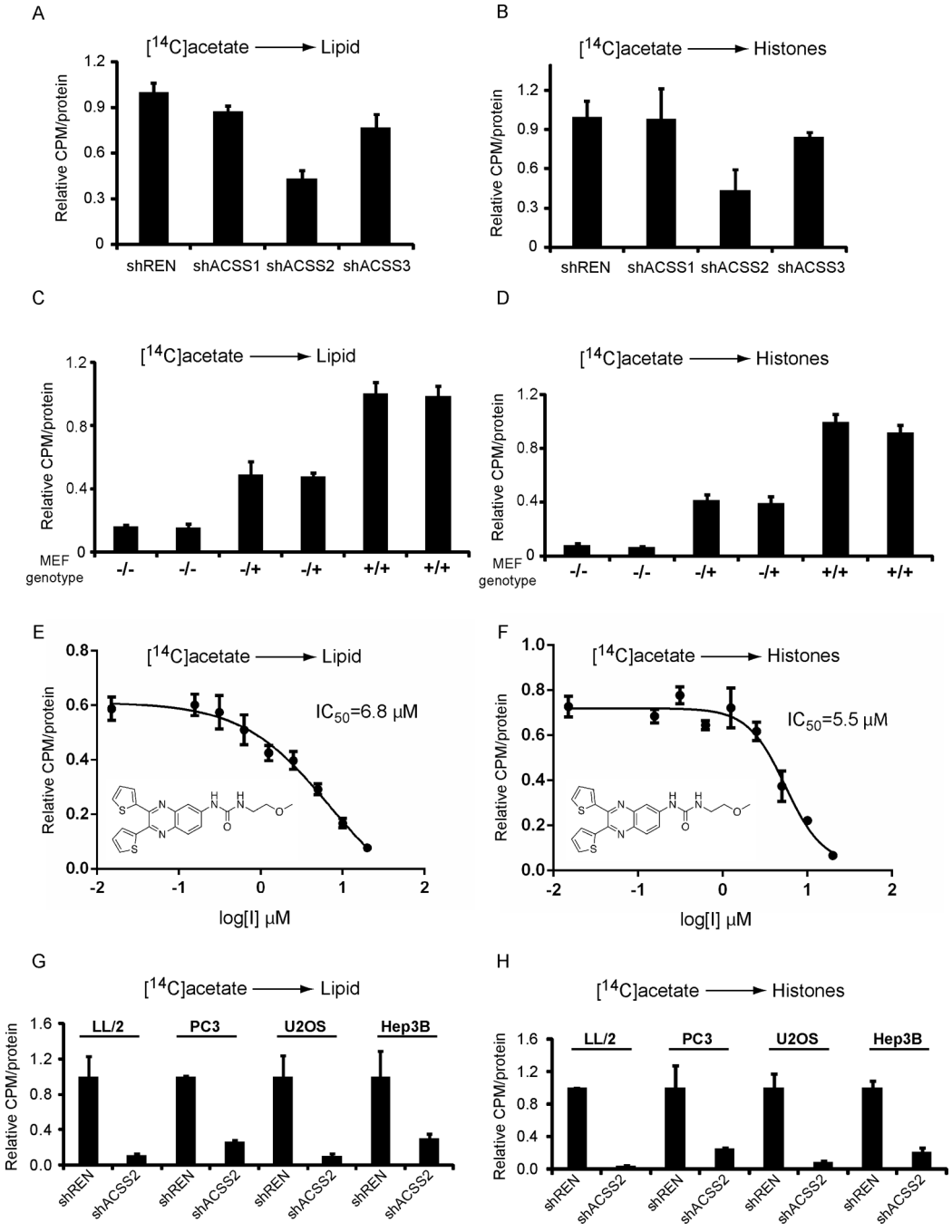

Figure 1. ACSS2 is the Major Enzyme Required for Incorporation of Acetate into Lipids and Histones

(A) HepG2 cells with constitutive shRNA knockdown of ACSS1, ACSS2, ACSS3, or control (REN) were assayed for their ability to utilize [^{14}C]acetate for lipid synthesis. Acetate must be converted to acetyl-CoA before it can be utilized as a metabolic substrate. Knockdown efficiency is shown in Figure S1.

(B) HepG2 cells with constitutive shRNA knockdown of ACSS1, ACSS2, ACSS3, or control (REN) were assayed for their ability to utilize [^{14}C]acetate for histone acetylation.

(C) Mouse embryonic fibroblasts (MEFs) were prepared from ACSS2 WT (+/+), heterozygous (−/+), and KO (−/−) mice, and assayed for their ability to incorporate [^{14}C]acetate into lipid. Note the −/− MEFs show very little [^{14}C]acetate incorporation into lipid fractions. ACSS2 protein levels in the MEFs are shown in Figure S1.

(D) MEFs of the indicated genotypes were assayed for their ability to utilize [^{14}C]acetate for histone acetylation. Note the −/− MEFs show very little [^{14}C]acetate incorporation into histones.

(E) ACSS2 is druggable. A high-throughput screen was conducted to identify small molecule inhibitors of the human ACSS2 enzyme (Experimental Procedures). The structure of one of the most potent and specific inhibitors, 1-(2,3-di(thiophen-2-yl)quinoxalin-6-yl)-3-(2-methoxyethyl)urea, is shown. This quinoxaline compound inhibited the ability of HepG2 cells to incorporate [^{14}C]acetate into lipids with IC_{50} = 6.8 μM.

(F) The quinoxaline was also able to inhibit HepG2 utilization of [^{14}C]acetate for histone acetylation with IC_{50} = 5.5 μM.

(G) Knockdown of ACSS2 in cancer cell lines significantly reduces acetate incorporation into lipids. [^{14}C]acetate incorporation into lipids was assayed in LL/2, PC3, U2OS, or Hep3B cancer cell lines harboring stable knockdown of ACSS2 or control (REN). Knockdown efficiency is shown in Figure S1. For each cell line, uptake amount was normalized against control.

(H) Knockdown of ACSS2 in cancer cell lines significantly reduces acetate incorporation into histones. [^{14}C]acetate incorporation into histones was assayed in cancer cell lines harboring stable knockdown of ACSS2 or control (REN).

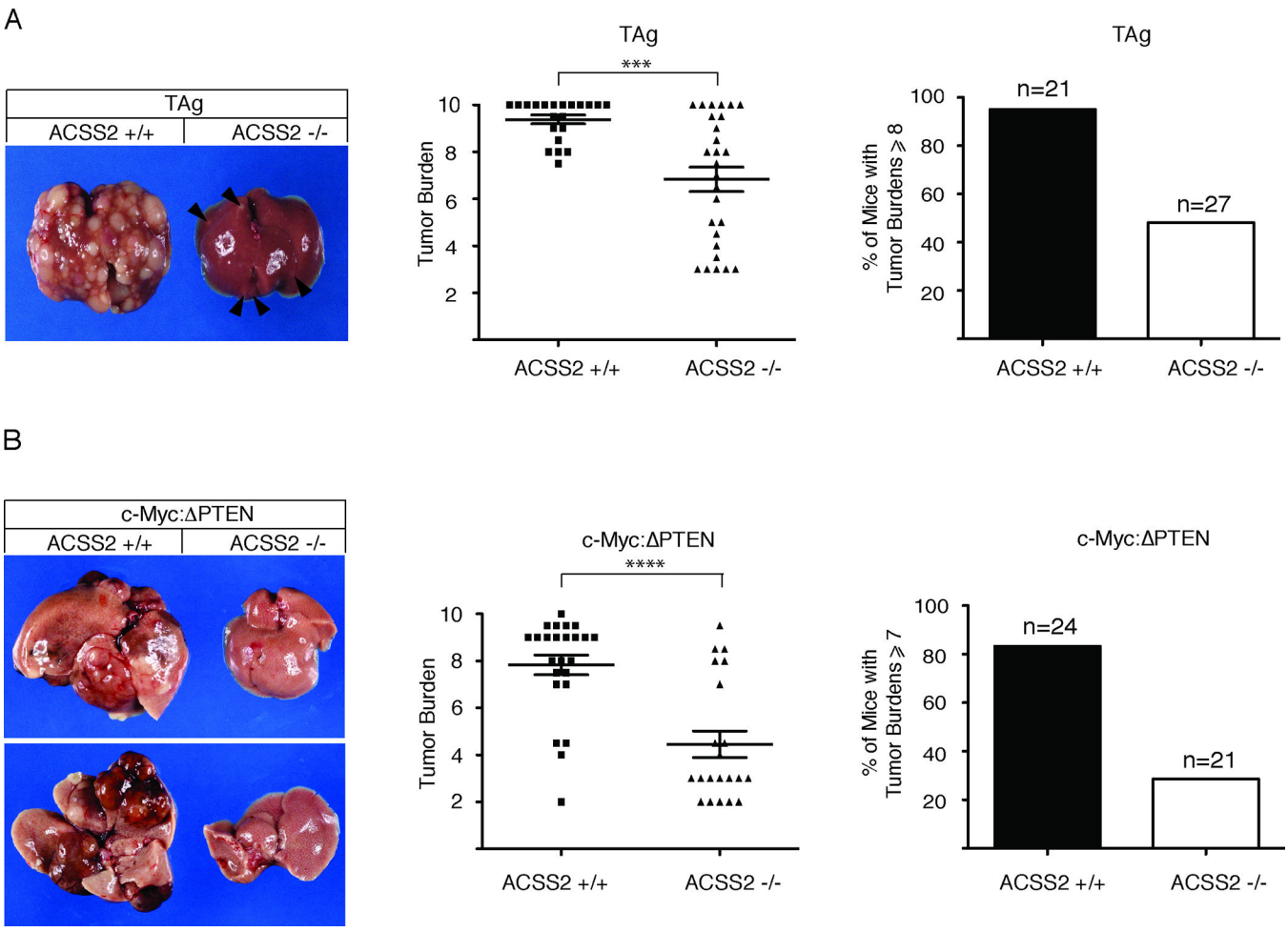

Figure 2. Loss of ACSS2 Suppresses Tumor Development

(A) Loss of ACSS2 reduces SV40-TAg-induced liver cancer. Left: Livers of mice treated with dox for 42–45 days to induce TAg-dependent tumorigenesis. The liver from an ACSS2+/+:TAg mouse with a tumor burden score of 9 (left) and the liver from an ACSS2−/−:TAg mouse with a tumor burden score of 4 (right). (Ventral View). Arrows denote small developing tumors. See Table S2 for detailed description of tumor scoring. Center: The distribution of tumor burden scores in livers of ACSS2+/+:TAg and ACSS2−/−:TAg mice after 42–45 days on dox (n=21 and 27 respectively). Loss of ACSS2-reduces the mean tumor burden score from 9.4 to 6.8 ($p = 0.0002$). Right: Graph showing % of ACSS2+/+:TAg and ACSS2−/−:TAg mice with tumor burden scores of 8 or greater after 42–45 days of dox-treatment (20/21 (95%) and 13/27 (48%) respectively). See also Figure S2.

(B) Loss of ACSS2 reduces the incidence of murine liver cancer caused by overexpression of c-Myc in conjunction with loss of PTEN (c-Myc:ΔPTEN). Left: Liver from a 6–7 month old ACSS2+/+:c-Myc:ΔPTEN mouse with a tumor burden score of 8 (left) adjacent to the liver from an ACSS2−/−:c-Myc:ΔPTEN mouse with a tumor burden score of 3 (right). Ventral view, top; dorsal view, bottom. See Table S2 for detailed description of tumor scoring. Center: The distribution of tumor burden scores in livers of ACSS2+/+:c-Myc:ΔPTEN and ACSS2−/−:c-Myc:ΔPTEN mice at 6–7 months of age (n= 24 and 21,

respectively). Loss of ACSS2 reduces the mean tumor burden score from 7.8 to 4.7 ($p < 0.0001$). Right: Graph showing % of ACSS2+/+:c-Myc:ΔPTEN and ACSS2−/−:c-Myc:ΔPTEN mice with tumor burden scores of ≥ 7 at 6–7 months of age (20/24 (83%) and 6/21 (29%), respectively). See also Figure S2.

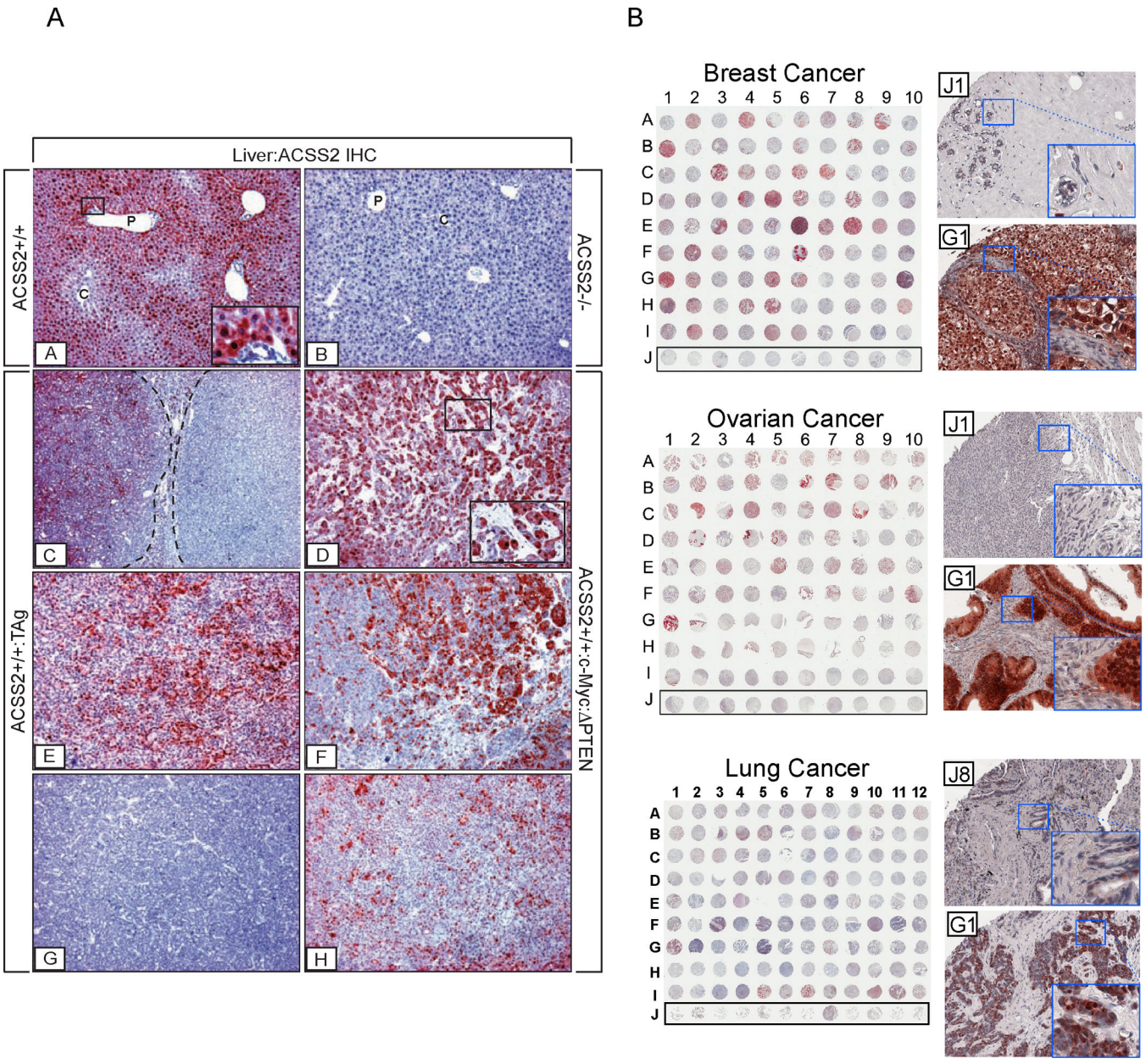

Figure 3. Immunohistochemical (IHC) Analysis of ACSS2 Expression in Tumors

(A) Expression patterns of ACSS2 protein in normal mouse liver and liver tumors. Insets: [A] ACSS2 IHC on WT liver showing regional expression of ACSS2 across the lobule. ACSS2 is localized to the nucleus/cytoplasm in zone 1 and 2 hepatocytes, but is largely absent from zone 3 hepatocytes and biliary cells. P, portal vein; C, central vein. [B] Complete absence of ACSS2 expression in liver of an ACSS2 −/− mouse. [C], [E], [G] Variability of ACSS2 expression in tumor-laden livers of ApoE-rtTA:TRE2-TAg mice provided with 10 μg/mL doxycycline for 42–45 days. [D], [F], [H] ACSS2 expression in c-Myc:ΔPTEN tumors. AEC chromagen (red); hematoxylin counterstain (blue). [A] ×60 mag, higher mag inset ×366; [B] ×60 mag; [C] ×36 mag; [D] ×60 mag, higher mag inset ×244; [E]–[H] ×60 mag.

(B) Survey of ACSS2 expression in human breast, ovarian, and lung tumors. IHC was carried out to assess ACSS2 protein expression in a panel of human breast, ovarian, and lung tumor sections in tissue microarray format. Row J denotes samples of normal, non-cancerous tissue. For each category of tumor, a higher magnification image of one representative example of staining in normal tissue, and one representative example of staining in a high ACSS2-expressing tumor, are shown to the right. Scoring of ACSS2 expression is these TMA samples is indicated in Table S5.

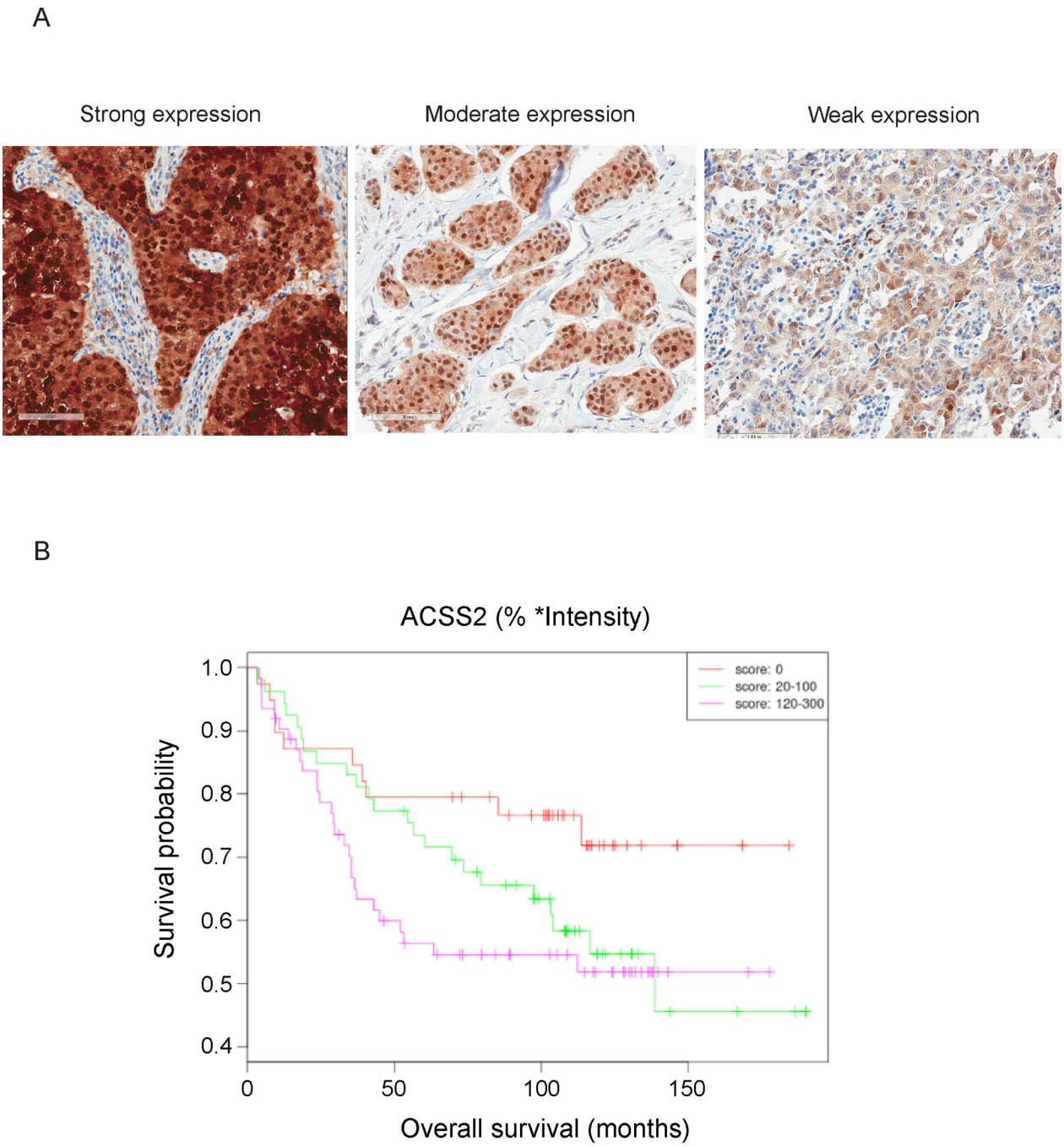

Figure 4. ACSS2 Expression in Triple Negative Breast Cancers

(A) Representative examples of high, medium, and low ACSS2 expression in triple negative breast cancers. The complete TMA staining is shown in Figure S3.

(B) High expression of ACSS2 was associated with poorer overall survival (p = 0.03).

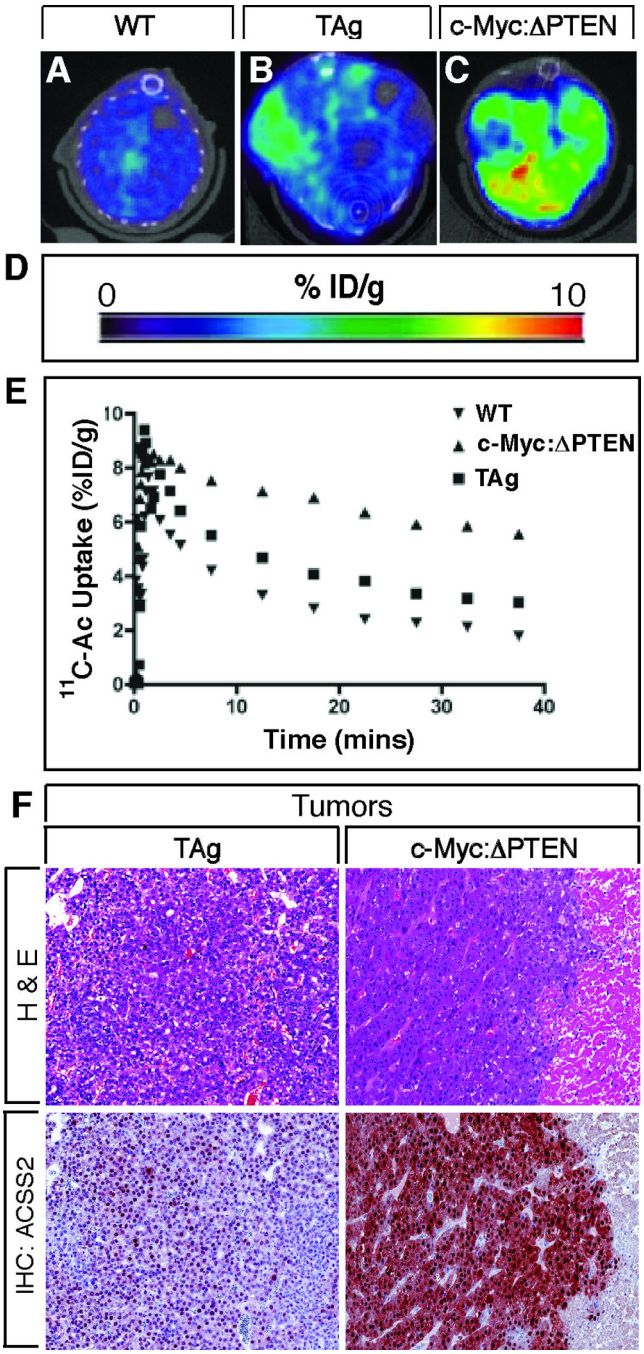

Figure 5. [^{11}C]Acetate Uptake Correlates with ACSS2 Expression in HCC Driven by TAg or Combined Overexpression of c-Myc and Loss of PTEN

(A–C) Combined [^{11}C]acetate PET/CT of WT (A), TAg (B) and c-Myc:ΔPTEN (C) mice (Transverse views).

(D) Scale (%ID/g) of avidity of [^{11}C]acetate uptake.

(E) Time activity curve (TAC) of 40 minute dynamic PET scan of [^{11}C]acetate uptake in WT, TAg and c-Myc:ΔPTEN mice shown in A–C.

(F) Photomicrographs (× 125 magnification) of H & E (top) and corresponding ACSS2 IHC (bottom) of tumors from TAg (left hand panels) and c-Myc:ΔPTEN (right hand panels) mice

shown in B and C. ACSS2 staining (red/brown color) is predominantly nuclear in the poorly differentiated tumor in the TAg mouse (left) but is both nuclear and cytoplasmic in the moderately differentiated trabecular HCC in the c-Myc:ΔPTEN mouse (right). See also Figure S4.

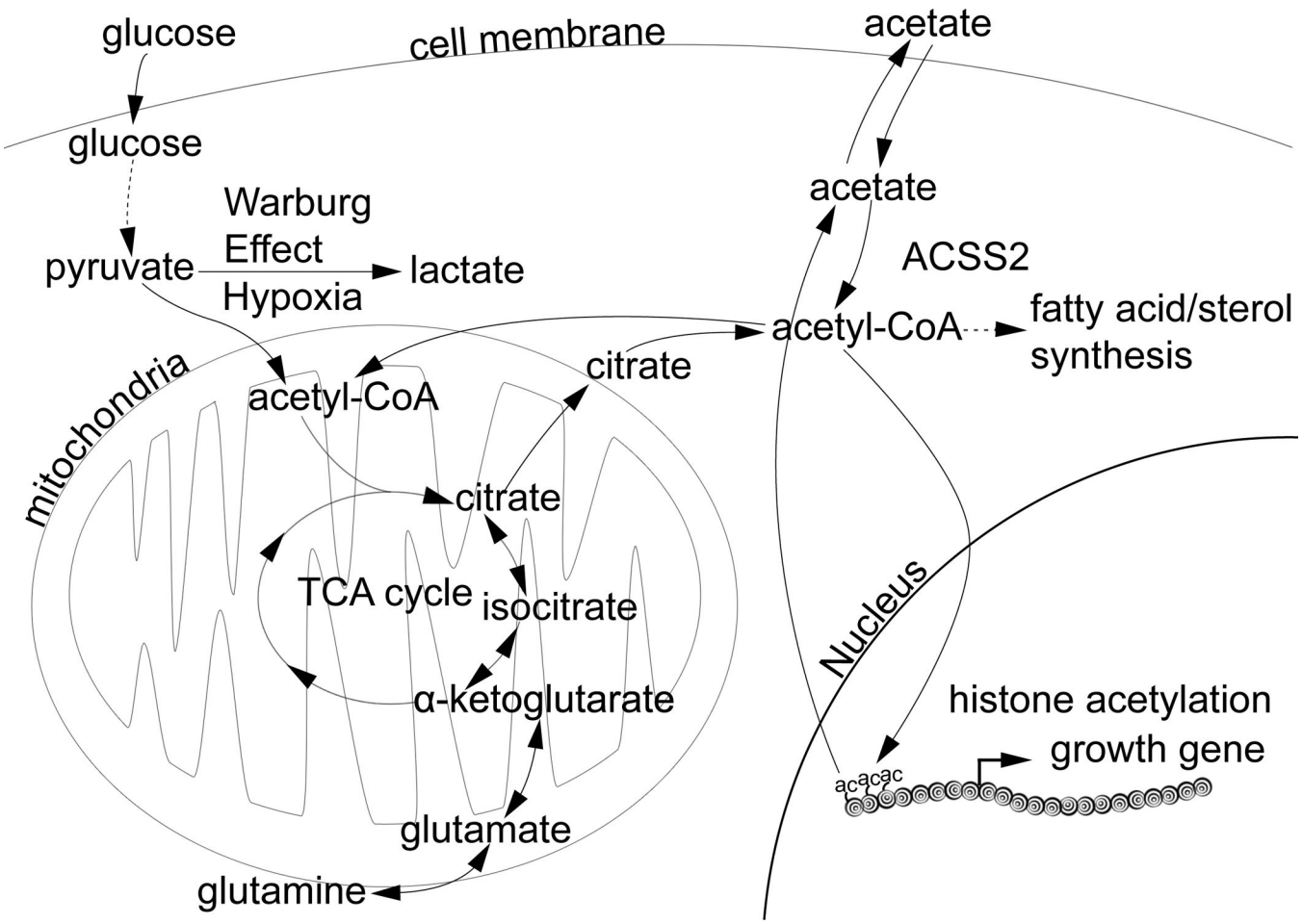

Figure 6. Acetate is a Critical Source of Acetyl-CoA for Certain Tumors

Schematic diagram depicting the pathways that synthesize and consume acetyl-CoA in mammalian cells. Hypoxic or highly glycolytic cancer cells preferentially shunt pyruvate to lactate, instead of to acetyl-CoA via the pyruvate dehydrogenase complex, raising the question of how such cells obtain sufficient quantities of acetyl-CoA. Among numerous metabolic functions, acetyl-CoA is used for fatty acid/sterol synthesis, histone acetylation, the synthesis of glutamate (related paper in this issue), or further oxidation via the TCA cycle for ATP synthesis. Glutamine can reportedly serve as a source of acetyl-CoA in cell culture studies. Acetate is an overlooked source of acetyl-CoA and can be produced as a result of histone or protein deacetylation, or from the action of acetyl-CoA thioesterase/hydrolase enzymes. The nucleocytosolic acetyl-CoA synthetase enzyme ACSS2 enables the recapture of acetate to acetyl-CoA that can subsequently be utilized for the indicated metabolic processes, all of which are expected to support tumor growth or survival.